Nearest neighbor interactions, habitat fragmentation, and the persistence of host-pathogen systems

Dominik Wodarz, Zhiying Sun, John W. Lau, and Natalia L. Komarova

Supplementary Information

Contents

Here we provide the details of several simulations and calculations described in the main text of the paper. We also provide an axiomatic description of the problem, where in many instances, instead of studying particular functional forms of host-pathogen interactions, we consider more general functions, which are assumed to satisfy certain biologically-motivated assumption. This type of approach provides a way to generalize conclusions of the analysis, and to ensure that these conclusions are not artifacts of the particular choice of functional forms.

1 Different formulations of enemy-victim dynamics

General description. In a very general case, the enemy-victim dynamics obey system (3) given in the main text. In our computer simulations, we consider several particular implementations of this general system with an explicit functional form for the enemy death rate:

$$\dot{x} = rx\tilde{f}(x,y,K) - \beta y\tilde{g}(x,y,K), \quad (1)$$

$$\dot{y} = \beta y\tilde{g}(x,y,K) - ay. \quad (2)$$

Here, $r\tilde{f} = f$, $\beta\tilde{g} = g$, where the functions f and g are as in equations (3) of the main text, and we require that $0 \leq \tilde{f} \leq 1$ and $0 \leq \tilde{g} \leq 1$. For convenience we factored out the constants r (the linear growth rate) and β (the exploitation rate).

Two different types of growth (the function $\tilde{f}$) were implemented:

(1): The standard logistic model, $\tilde{f} = 1-(x+y)/K-d/r$, where the population grows exponentially, and the growth saturates as the population size approaches the effective carrying capacity, $K(1-d/r)$.

(2): A different law: $\tilde{f} = (1-(x+y)/K)/(x+\eta)-d/r$. This means that the victims grow exponentially at low numbers, then the growth slows down to become linear, and finally, the growth saturates at a carrying capacity.

Also, two different models were implemented for the exploitation function:

(1): The exploitation happens proportional to the density of victims: $\tilde{g} = x/K$. This is a rescaling of a standard Lotka-Volterra model.

(2): The exploitation rate is a growing function of victims which reaches saturation for large population sizes: $\tilde{g} = x/(x+y+\epsilon)$. This is similar to the Beddington-DeAngelis functional response in ecology [2, 5], or a generalization of the "frequency dependent" infection incidence in epidemiology [11].

These functional forms, used in combination, gave rise to four different models of enemy-victim interactions that we presented as our case studies. We list them below:

- Model 1: $\dot{x} = rx(1-(x+y)/K) - dx - \beta xy/K$, $\dot{y} = \beta xy/K - ay$.
- Model 2: $\dot{x} = rx(1-(x+y)/K) - dx - \beta xy/(x+y+\epsilon)$, $\dot{y} = \beta xy/(x+y+\epsilon) - ay$.
- Model 3: $\dot{x} = rx(1-(x+y)/K)/(x+\eta) - dx - \beta xy/K$, $\dot{y} = \beta xy/K - ay$.
- Model 4: $\dot{x} = rx(1-(x+y)/K)/(x+\eta) - dx - \beta xy/(x+y+\epsilon)$, $\dot{y} = \beta xy/(x+y+\epsilon) - ay$.

The equilibria. Systems of type (1-2) commonly have the following equilibria:

- the trivial equilibrium, $x = y = 0$, which is unstable;
- the enemy extinction equilibrium, characterized by $x = x^{(0)} = K$, $y = y^{(0)} = 0$;
- the coexistence (or the internal) equilibrium, $x = x^{(1)} > 0$, $y = y^{(1)} > 0$.

The long-term dynamics of the system is defined by the latter two equilibria. Extinction events cannot be explained by deterministic ODEs alone, and come about as a result of stochastic dynamics, as explained below.

2 Agent-based models of enemy-victim interactions

Agent-based models are models where one tracks the fate of individuals, enemies and victims. The dynamics of the individuals is described by microscopic update rules.

2.1 Model formulation

We set up a square $N \times N$ grid, where each location can be either empty, or occupied by a victim or an enemy. We define the neighborhood of a given cell to be (i) all cells in the mass-action case, (ii) the 8 nearest neighbors in the spatial case. We define constants R, B, and A as the rates at which reproduction, exploitation and death events are attempted (but not necessarily performed, the full probabilities are given by the rules below). We assume that the ratios of rates are preserved: $R/B = r/\beta$ and $A/B = a/\beta$. In a fixed time-interval, the grid is updated $N \times N$ times. We implement the following microscopic update rules. Pick a location in the grid at random.

- If the location is empty, no changes occur.
- If the location is occupied by a victim, a reproduction occurs with probability $R\tilde{f}(X, Y, K)$, where and X and Y are the numbers of victims and enemies in the neighborhood of the chosen location. As the result of the reproduction, the victim places its offspring in a randomly chosen empty spot in its neighborhood. By definition, if $X + Y = K$ (that is, no empty spots exist in the neighborhood), $\tilde{f}(X, Y, K) = 0$, and reproduction will not occur.
- If the location is occupied by an enemy, death occurs with probability A (the spot becomes empty). Alternatively, an exploitation event occurs with probability $B\tilde{g}(X, Y, K)$. No changes occur with probability $1 - A - B\tilde{g}(X, Y, K)$.

The agent-based algorithm presented here is a generalization of the algorithm that appears in figure 1 of the main text. It helps create an agent-based simulation equivalent to the ODE model (1-2) with any given choices of the functions $\tilde{f}$ and $\tilde{g}$. This algorithm was implemented in simulations of figure 5 of the main text.

For the mass-action system, the equations for average quantities governed by the above rules can be derived. They are given by

$$d\langle X\rangle/dt = R(\langle X\tilde{f}(X, Y, K)\rangle - B\langle Y\tilde{g}(X, Y, K)\rangle, \quad (3)$$

$$d\langle Y\rangle/dt = B\langle Y\tilde{g}(X, Y, K)\rangle - A\langle Y\rangle, \quad (4)$$

where the angular brackets denote the expected values. Unless functions $\tilde{f}$ and $\tilde{g}$ are constants, the above equations involve higher moments, and as

with most nonlinear stochastic processes, the system is not closed. However, if we simply decouple the equations by replacing $\langle X\tilde{f}(X,Y,K)\rangle \rightarrow \langle X\rangle\tilde{f}(\langle X\rangle,\langle Y\rangle,K)$ and $\langle Y\tilde{g}(X,Y,K)\rangle \rightarrow \langle Y\rangle\tilde{g}(\langle X\rangle,\langle Y\rangle,K)$, we obtain equations similar to (1-2). The two systems become exactly the same after we rescale time $t \rightarrow tB/\beta$.

The decoupling procedure used here can be regarded as the simplest type of a moment closure technique, where we assume that the covariance of X and Y is small. The resulting system of ODEs (system (1-2)) does not exactly describe the behavior of the means (system (3-4) does), but is known to have similar properties in many contexts, especially when steady-states are concerned. A more precise approximation of the mean behavior can be obtained when decoupling by a moment closure technique is performed at higher orders, see e. g. [10].

A typical agent-based simulation performed in this paper uses a 30×30 grid. The initial configuration contains a 5×5 square filled with enemies in the middle, immersed in a bigger (13×13) square containing victims, with the rest of the grid being empty.

2.2 Alternative methodologies for studying agent-based model dynamics.

In this paper, we considered an agent-based model where individuals can only interact with their nearest neighbors, i.e. interactions are spatially restricted. In the past, techniques have been developed to describe spatial systems of this nature with ordinary differential equations (ODEs), using pair approximation methods [6, 14, 12, 13, 4]. We implemented those methods but found that this does not provide a sufficiently good description of the outcomes and the dynamics. The dynamics tended to fall somewhere between the outcome observed in the mass-action ODE (that is, the ODE describing the system where mass-action rules apply over the whole domain) and the true spatial dynamics observed in the simulations of the agent-based model. In fact, in many cases the pair approximation only provided a small correction to a mass-action description, failing to describe the dynamics of a spatially-restricted system. More details about the accuracy of the pair approximation method will be provided elsewhere [16]. Hence, this method was not used to study the spatial system and will not be further discussed. Instead, we obtained sufficient understanding of the spatial system through a

combination of extensive numerical simulations and the local ODE analysis, as explained in the main text.

2.3 Time to extinction

In this section we demonstrate that the graphs of figure 2 of the main text do not change significantly as we change the cut-off time. Figure S1 presents the extinction/persistence plots that were generated for two different cut-off times, $T = 3 \times 10^5$ (a) and $T = 3 \times 10^7$ (b). The first of these graphs is identical to that appearing in the main paper, figure 2a(ii), and is given for comparison. The graph in figure S1(b) corresponding to longer cut-off times only includes the relevant parts of the parameter space where we observe existence/persistence boundaries. This was done to reduce the computational cost of these very long simulations. Comparing the two graphs in figure S1 we can see that the location of the boundaries does not depend significantly on the cut-off time. This illustrates the statement that in the blue region of coexistence, the system is found in a long-lived quasi-steady state.

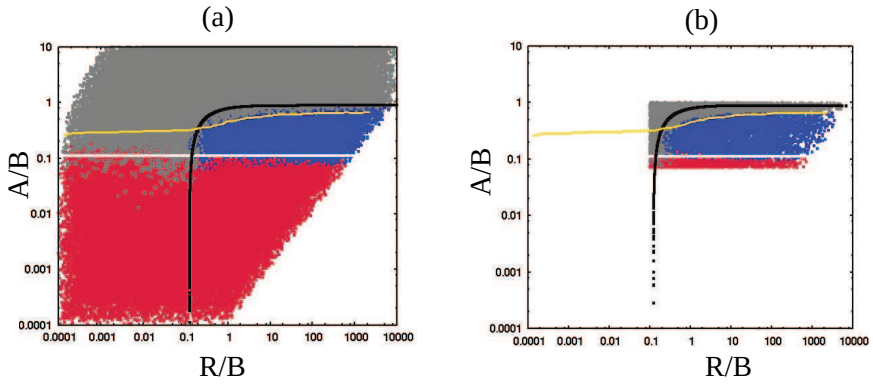

Figure S1: Agent-base model simulations performed for two different cut-off times: $T = 3 \times 10^5$ (a) and $T = 3 \times 10^7$ (b). The figure in panel (a) is identical to figure 2a(ii) of the main text. Each point represents the outcome of a single run. Red indicates extinction of host and pathogen, blue indicates coexistence, and gray indicates persistence of the host in the absence of the pathogen. Above the white and below the black lines, the local equilibrium number of hosts and pathogens, respectively, is greater than approximately one. Above the yellow line, the pathogen fails to invade. The parameters are as in figure 2a(ii) of the main text.

3 Metapopulation models of enemy-victim interactions

3.1 Model formulation

The other type of models that we use is metapopulation models. Metapopulation models consist of individual patches, such that the rules specified by equations (1-2) apply in each patch, and the value K corresponds to the local carrying capacity, $K \to K_{patch}$. The individual patches communicate with each other, such that enemies and victims can migrate to the neighboring patches with certain rates, which we denote μ_x and μ_y for victims and enemies respectively. Let us denote by x_i and y_i the number of victims and enemies in patch i, and introduce the short-hand notation, $g_i = g(x_i, y_i, K_{patch})$, $f_i = f(x_i, y_i, K_{patch})$. The deterministic spatial system has the following form:

$$\dot{x}_i = r x_i \tilde{f}_i - \beta y_i \tilde{g}_i + \frac{\mu_x}{2}(x_{i-1} - 2x_i + x_{i+1}), \quad (5)$$

$$\dot{y}_i = \beta y_i \tilde{g}_i - a y_i + \frac{\mu_y}{2}(y_{i-1} - 2y_i + y_{i+1}), \quad 2 \leq i \leq n-1, \quad (6)$$

This system is equipped with the boundary conditions, where species in patches 1 and n only migrate to sites 2 and $n-1$ respectively. System (5-6) is a generalization of system (2) of the main text. In the latter system, we considered a particular model of host-pathogen interaction. In system (5-6) we study more general enemy-victim dynamics. Methods developed here for this system were used in simulations of figure 4 of the main text.

As with the stochastic process described above being a generalization of the agent-based model used in the main body of the paper, the metapopulation model of system (5-6) is a generalization of the metapopulation model used in the main body of the paper.

The stochastic simulation is set up as a standard Gillespie algorithm [7, 8]. The simulation proceeds as a sequence of time-steps. At each time-step, j, let us denote the local numbers of victims and enemies as $x_i^{(j)}, y_i^{(j)}$. The different terms in system of equations (5-6) define the relative probability weights of different events that could happen at the next update. Let us form the sum

$$\Sigma^{(j)} = \sum_{i=1}^{n} \left(r x_i^{(j)} \tilde{f}_i^{(j)} + \beta y_i^{(j)} \tilde{g}_i^{(j)} + a y_i^{(j)} + \mu_x x_i + \mu_y y_i \right).$$

Then the probability that at patch i, an enemy will die is given by

$$ay_i^{(j)}/\Sigma^{(j)},$$

the probability that at patch i, an exploitation event will take place is given by

$$\beta x_i^{(j)}\tilde{g}_i^{(j)}/\Sigma^{(j)},$$

the probability that a victim will migrate from patch i to patch $i+1$ is given by

$$(\mu_x/2)x_i^{(j)}/\Sigma^{(j)},$$

and so on. Guided by these probabilities, we pick the next event and update the system accordingly. For example, if the next event is a death of an enemy in patch i, we take $y_i^{(j+1)} = y_i^{(j)} - 1$, and keep the rest of the variables the same. If the next event is an exploitation event in patch i, we take $y_i^{(j+1)} = y_i^{(j)} + 1$, $x_i^{(j+1)} = x_i^{(j)} - 1$, and keep the rest of the variables the same. If the event is a migration of a victim from patch i to patch $i+1$, we take $x_i^{(j+1)} = x_i^{(j)} - 1$, $x_{i+1}^{(j+1)} = x_{i+1}^{(j)} + 1$. Finally, we determine the length of the time-step between state $(j+1)$ and state (j) from the exponential distribution with the constant $\sigma^{(j)}$: $P(\tau) = \Sigma^{(j)}e^{-\Sigma^{(j)}\tau}$.

A note on the migration rates: in the agent-based models implemented here, the agents do not move from spot to spot, and only spread by proliferation. In contrast, in the metapopulation models, enemies and victims migrate to the two nearest patches with a rate μ_x and μ_y, respectively (moving through space by individuals placing their offspring to the nearest neighboring spots is not a natural choice under the metapopulation framework). In the metapopulation model, we assume that the migration rates $\mu_x = \mu_y$. In this case, no additional asymmetries are introduced that are not found in the agent-based model.

A typical simulation performed in this paper contains $n = 100$ patches, with carrying capacity $K_{patch} = 100$. The initial configuration consists of one patch in the middle containing $0.7K_{patch}$ victims and $0.3K_{patch}$ enemies, surrounded by 10 patches (5 on each side) containing only victims at carrying capacity. The rest of the patches are empty ($x_i = y_i = 0$).

A "mass-action" variant of the metapopulation is obtained in the following way: we consider only 1 patch, with $K = nK_{patch}$, and use the Gillespie algorithm corresponding to its local dynamics. For such simulations, the initial condition used is $0.7K$ victims and $0.3K$ enemies.

3.2 1D and 2D models

Most of the metapopulation simulations presented in the paper were performed for metapopulations consisting of a one-dimensional array of patches, where migration was allowed between adjacent patches. The question arises whether the behavior would change in a two-dimensional array of metapopulation patches.

Intuitively, in the agent-based model we expect the 2D system to behave very differently compared to a 1D system. A 2D habitat in an agent-based model provides refuge possibilities for the hosts which are lacking in a 1D chain of agents. A 1D setting does not easily allow persistence, since susceptible agents may not escape infecteds.

It is interesting that the relationship between 1D and 2D scenarios is quite different for the metapopulation. There, it turns out that the observed behavior in a 2D metapopulation is very similar to that in a 1D metapopulation. This is demonstrated in figure S2, which was created for a two-dimensional 10×10 array of metapopulation patches. This figure should be compared with figure 7a(ii) of the main text, created for a 1D array of 100 metapopulation patches. The figures show persistence/existence outcomes for the metapopulation system governed by equations (5-6) (Model 1). We observe nearly identical behavior in one and two dimensions. Unlike in agent-based models, the dimensionality of metapopulations does not make a significant difference.

The reason for this difference between agent-based models and metapopulations is as follows. In the agent-based model, one spot corresponds to a single individual. In the metapopulation model, a patch corresponds to a local population evolving according to mass-action rules. Effectively, the local mass-action dynamics within each patch act like an extra dimension. Therefore, a 1D chain of metapopulations does not possess the same degree of spatial restriction as a 1D row of agents in an agent-based model.

There is one slight difference between the 2D metapopulation figure plot in figure S2 and the 1D figure 7a(ii) in the main text. In the 1D metapopulation plot, there is a small region of coexistence below the white line (corresponding to $S^{(1)} = 1$). This region is almost non-existent in the 2D figure. The reason for the persistence in the 1D metapopulation is a formation of non-equilibrium macroscopic structures along a 1D chain of 100 patches. In the 2D metapopulation, these structures have a harder time forming because the linear size of a 2D array of patches in this case is only 10. For larger 2D

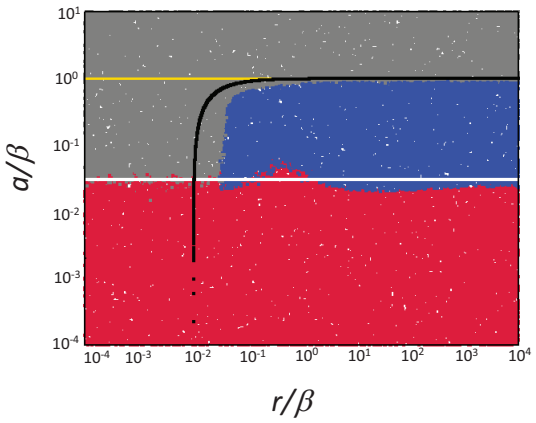

Figure S2: Two-dimensional metapopulation model, to be compared with 1D metapopulation model, figure 7a(ii) in the main text. Each point represents the outcome of a single run. Red indicates extinction of host and pathogen, blue indicates coexistence, and gray indicates persistence of the host in the absence of the pathogen. Above the white and below the black lines, the local equilibrium number of hosts and pathogens, respectively, is greater than approximately one. Above the yellow line, the pathogen fails to invade. There are $n = 100$ patches arranged in a 10×10 square array. The rest of the parameters are as in figure 7a(ii) of the main text.

metapopulations, these macroscopic structures will form in 2D like they do in 1D.

4 Coexistence threshold in metapopulations

In this section we discuss the meaning of the threshold given by the local equilibrium population equal to one. The theoretical results below are derived for a metapopulation model with large diffusion. In the main paper, they are confirmed numerically for the agent-based model in a continuous habitat.

4.1 Theoretical considerations

We start with a population that undergoes a nonlinear birth-death process, and can be described by a stochastic variable i. Host-pathogen models considered in this paper are slightly more complicated because they are described

by two stochastic variables. The arguments presented here can be generalized to such systems, and the results are confirmed by numerical experiments, see below. The infinitesimal probabilities of change are given by

$$P^{\uparrow}(i) \equiv Prob(i \to i+1) = \lambda(i)\Delta t,$$
$$P^{\downarrow}(i) \equiv Prob(i \to i-1) = \mu(i)\Delta t,$$
$$Prob(i \to i) = 1 - Prob(i \to i+1) - Prob(i \to i-1).$$

We assume that

$$\lambda(0) = \mu(0) = 0. \tag{7}$$

We further assume the existence of a threshold value of i, $\bar{X}$, such that the following holds:

$$\begin{aligned} i < \bar{X} &\Rightarrow P^{\uparrow}(i) > P^{\downarrow}(i) \\ i > \bar{X} &\Rightarrow P^{\uparrow}(i) < P^{\downarrow}(i) \\ i = \bar{X} &\Rightarrow P^{\uparrow}(i) = P^{\downarrow}(i) = 1/2. \end{aligned}$$

Then the mean population size will be around $\bar{x}$. However, the smaller the value of $\bar{x}$, the faster fluctuations will lead to a stochastic extinction of this system.

Next, let us assume a subdivision of this system into n patches (a metapopulation model). In each patch, if it is isolated from others, we have a birth-death process defined similarly to the one above, except the threshold value $\bar{X}$ is replaced by a scaled-down threshold,

$$\bar{x} = \frac{\bar{X}}{n}.$$

Denoting the local probabilities by lower-case letters, we have

$$\begin{aligned} i < \bar{x} &\Rightarrow p^{\uparrow}(i) > p^{\downarrow}(i) \\ i > \bar{x} &\Rightarrow p^{\uparrow}(i) < p^{\downarrow}(i) \\ i = \bar{x} &\Rightarrow p^{\uparrow}(i) = p^{\downarrow}(i) = 1/2. \end{aligned}$$

If the patches are disconnected, the expected value of the total population size will again be $\bar{X}$, but the system will be even less stable because the local threshold values are smaller than in the undivided system.

If we assume a certain amount of migration among patches, the process stops being one-dimensional. A simple description is impossible. We know

from numerical simulations that such systems tend to be more stable than the disconnected ones. The amount of fluctuations decreases with increasing migration rate and increasing n.

To make the description possible, we can make an assumption of very large diffusion. This means that the individuals in the patches are subject to migration, and the time-scale of migration is a lot faster than that of the birth-death process. In the limit of infinite migration, we can assume that the population has a chance to diffuse and reach a uniform state after each birth or death event. This allows us to use a one-dimensional description once more.

Suppose the total population size is i. Then each patch contains on average i/n individuals. Non-integer values however are not allowed, which means that if $i/n \notin \mathbb{N}$, then all patches will contain either $k \leq i_l \equiv [i/n]$ individuals or $k \geq i_h \equiv [i/n] + 1$ individuals, where the square brackets denote rounding down. Let us denote by $\phi(k)$ the relative probability that an event will happen in a patch with k individuals. The functional form of $\phi(k)$ is unimportant as long as

$$\sum_{k \leq i_l} \phi(k) > 0, \quad \sum_{k \geq i_h} \phi(k) > 0,$$

and

$$\phi(i_l) \gg \phi(i_l - 1) \gg \phi(i_l - 2) \ldots, \quad \phi(i_h) \gg \phi(i_h + 1) \gg \phi(i_h + 2) \ldots. \quad (8)$$

The former condition states that there will be states with the number of individuals both greater and smaller than i/n. The latter condition states that deviations from a uniform distribution of individuals are small. This is guaranteed by a large diffusion in the system. In fact, in the limit of infinite diffusion we can assume $\phi(k) = 0$ with $k > i_h$ or $k < i_l$.

We can write down the probability for the system to increase or decrease the number of individuals:

$$\begin{aligned} P^{\uparrow}(i) &= \sum_{k \leq i_l} \phi(k) p^{\uparrow}(k) + \sum_{k \geq i_h} \phi(k) p^{\uparrow}(k), \\ P^{\downarrow}(i) &= \sum_{k \leq i_l} \phi(k) p^{\downarrow}(k) + \sum_{k \geq i_h} \phi(k) p^{\downarrow}(k). \end{aligned}$$

Let us investigate the properties of a state where $i \approx \bar{X}$. Let us suppose that $\bar{x} \notin \mathbb{N}$. Then we have the following patterns.

- Suppose that $\bar{x} > 1$. Then all values of i can be divided into three groups: Group 1 consists of all i such that $i_h, i_l > \bar{x}$. In the limit of large diffusion, for this group we have $P^{\uparrow}(i) > P^{\downarrow}(i)$, see inequality (8). Group 2 consists of values of i such that $i_h, i_l < \bar{x}$ (this group consists of values $i < n$). For this group $P^{\uparrow}(i) < P^{\downarrow}(i)$. Group 3 consists of all i such that $i_l < \bar{x}$, $i_h > \bar{x}$. Group 3 is an attractive set in the following sense. If the system is in a state in group 1, it will on average decline until it enters a state in group 3. If on the other hand the system is in state 2, it will increase until it reaches a state in group 3.

- If $\bar{x} < 1$, group 2 does not exist, and group 3 has $i_l = 0$ and $i_h = 1$. We have $p^{\downarrow}(0) = p^{\uparrow}(0) = 0$ (condition (7)). Therefore for group 3, we have $P^{\uparrow} = \sum_{k\geq 1} \phi(k) p^{\uparrow}(k) < P^{\downarrow} = \sum_{k\geq 1} \phi(k) p^{\downarrow}(k)$, which follows from the fact that $i_h = 1 > \bar{x}$. This means that as the number of individuals falls below $\bar{X}$, it will on average continue to decrease.

This argument explains the fundamental difference between systems with $\bar{x} > 1$ and $\bar{x} < 1$. In the former case, if the fluctuations are not too large, the system will have a nonzero quasi-steady state (fluctuations can be reduced by increasing the number of patches, n). In the latter case, no such quasi-steady state exists.

4.2 Numerical validation

This argument presented for simplicity for birth-death processes, can be extended to enemy-victim (e.g. host-pathogen) systems. In figure S3 we show the results of a numerical implementation of a metapopulation system, with the stochastic host-pathogen dynamics is modeled after equations (5-6), Model 1, with a very large migration rate. The parameters r, β, μ, and K_{patch} were kept constant, and a changed. To simulate the limit of infinite migration, the following algorithm was employed. After each division/death/infection update performed in accordance with the Gillespie method, we randomly redistributed all the individuals among the patches, resulting in a nearly uniform distribution. For each value of a/β, we performed on average 600 (and at least 200) simulations. The outcome by the fixed cut-off time t (coexistence of extinction) was recorded, and then the percentage of runs that ended up in persistence/extinction states were plotted. As the value of a/β changes from 0 to 0.05, the system crosses the threshold imposed by the condition $S^{(1)} = 1$. Since $S^{(1)} = aK_{patch}/\beta$, this

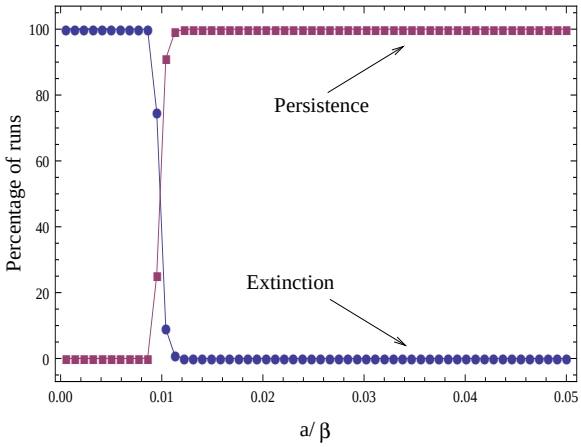

Figure S3: The threshold effect of crossing the $S^{(1)} = 1$ line. For a host-pathogen metapopulation system with large diffusion, the percentage of runs is plotted that ended up in extinction (persistence), for each value of parameter a. The other parameters are: $\beta = 1$, $K_{patch} = 100$, $n = 100$, $r = 100$, and the cut-off time of the simulations is $t = 3 \times 10^5$.

threshold is given by $a/\beta = 0.01$ for the given parameter values. As we can see from the graph, for $a/\beta < 0.01$, the overwhelming majority of the runs resulted in extinction, and for $a/\beta > 0.01$, in persistence, with a very sharp transition between the two states.

The graphs of figure S4 show how the above theory applies to metapopulations with finite migration rates. In this figure, we ran simulations and recorded extinction (red) and persistence (blue) outcomes much like in figure 7a(ii) of the main text, but the parameters that we varied were a (the vertical axis) and K_{patch} (horizontal axis). The rest of the parameters were kept constant, including the total population size nK_{patch} (such that n is different for different runs). The two figures S4(a) and (b) differ by the choice of the migration parameter, $\mu = 1$ for figure (a) and it is $\mu = 10$ for figure (b). The gray line represents the theoretical threshold $S^{(1)} = 1$, which corresponds to $a/\beta = 1/K_{patch}$. We observe the following patterns:

- For finite migration rates, there is an area corresponding to $S^{(1)} > 1$ which is characterized by population extinction.
- As μ increases, the existence threshold approaches the theoretically predicted threshold $S^{(1)} = 1$. This is predicted by the theory above.

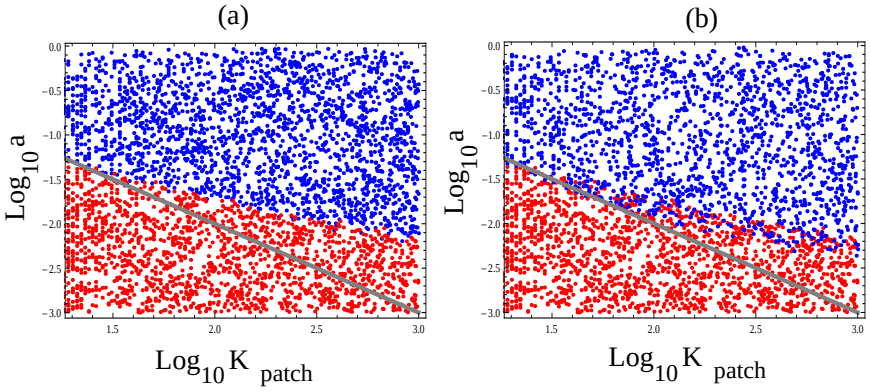

Figure S4: Metapopulations with a finite migration rate: the threshold effect of crossing the $S^{(1)} = 1$ line. Each point represents the outcome of a single run. Red indicates extinction of host and pathogen and blue indicates coexistence. The gray line corresponds to $S^{(1)} = 1$. The parameters K_{patch} and a are varied. The total size of the metapopulation is kept constant, $nK_{patch} = 10^4$. The migratio nrate is given by (a) $\mu = 1$ and (b) $\mu = 10$. The other parameters are: $\beta = 1$, $r = 100$. For cut-off time of the simulations, see legend of figure 7 in the main text.

- For each migration rate, the proximity to the theoretical threshold is closer for a larger number of patches (which corresponds to smaller K_{patch}). This is also predicted as a larger number of patches decreases fluctuations in the system.

We conclude that the theory presented here is applicable to simulations with finite migration parameters, as long as the number of patches is not too small.

5 General conditions required for space to promote extinction

A central message of this paper is that under certain circumstances, mass-action dynamics can promote coexistence. In other words, it can happen that a mass-action systems exhibits a stable coexistence solution, while in the spatially distributed system with the same parameters no coexistence is observed, and either the enemies, or both species go extinct.

As mentioned before, coexistence is more likely for larger values of the equilibrium $x^{(1)}$. These values, in turn, are defined by the system parameters,

and in particular, by the parameter K. This helps us explain how spatial interactions (translated into the effective carrying capacity, K) can influence the coexistence of enemies and victims.

If we can show that in a given model, the mass-action equilibrium value for x is larger than that in a spatially restricted system, then in such a model mass-action rules will have a tendency to promote coexistence of the species. Therefore, in order to explain the role of space for the coexistence of species, we must investigate how the equilibrium $x^{(1)}$ depends on the effective carrying capacity, K. In what follows, we address the general question: in what types of enemy-victim interactions does $x^{(1)}$ negatively correlate with K?

Coexistence solution. The dynamics of enemies and victims is described by the general system given by equation (3) of the main text, with the following assumptions (see also [1]):

$$\frac{\partial f}{\partial x} \leq 0, \quad \frac{\partial f}{\partial y} \leq 0, \quad \frac{\partial f}{\partial K} > 0, \tag{9}$$

$$\frac{\partial g}{\partial x} > 0, \quad \frac{\partial g}{\partial y} \leq 0, \tag{10}$$

$$\frac{\partial F}{\partial g} \geq 0. \tag{11}$$

A nontrivial fixed point corresponding to the coexistence solution is given by the system,

$$xf(x, y, K) - yg(x, y, K) = 0, \tag{12}$$

$$F(g(x, y, K), x, y) = 0. \tag{13}$$

Let us assume that equation

$$F(\gamma, x, y) = 0$$

has a solution, $\gamma(x, y)$. This describes the relationship between the exploitation function, $g(x, y, K)$, and the variables, (x, y), at equilibrium. Substituting this solution into the first equilibrium equation, we obtain

$$xf(x, y, K) - y\gamma(x, y) = 0. \tag{14}$$

This implicitly defines the function $y = \tilde{y}(x, K)$. Finally, the steady-state solution can be obtained: the steady-state level $x = x^{(1)}$ is given by equation

$$F(\gamma(x, \tilde{y}(x, K)), x, \tilde{y}(x, K)) = 0, \tag{15}$$

and $y^{(1)} = \tilde{y}(x^{(1)}, K)$.

Stability of the coexistence solution. Let us investigate stability of solution $(x^{(1)}, y^{(1)})$. The Jacobian of the system is given by

$$J = \begin{pmatrix} f + xf_x - yg_x & xf_y - g - yg_y \\ y\frac{\partial F}{\partial g}g_x + y\frac{\partial F}{\partial x} & F + y\frac{\partial F}{\partial g}g_y + y\frac{\partial F}{\partial y} \end{pmatrix}$$

Here we used the short-hand notation $f_x = \frac{\partial f}{\partial x}$, and similarly with f_y, g_x and g_y. All the functions are assumed to be evaluated at the steady state, $(x^{(1)}, y^{(1)})$. Note that $F = 0$ at the steady state. A necessary condition of stability of the solution $(x^{(1)}, y^{(1)})$ is that $Det(J) \geq 0$. This condition is equivalent to :

$$Det(J) = (f+xf_x-yg_x)(y\frac{\partial F}{\partial g}g_y+y\frac{\partial F}{\partial y})-(y\frac{\partial F}{\partial g}g_x+y\frac{\partial F}{\partial x})(xf_y-g-yg_y) \geq 0.$$

Let us differentiate equation (12) with $y = \tilde{y}(x, K)$, with respect to x:

$$f + xf_x + xf_y\frac{\partial \tilde{y}}{\partial x} - \frac{\partial \tilde{y}}{\partial x}g - \tilde{y}g_x - \tilde{y}g_y\frac{\partial \tilde{y}}{\partial x} = 0.$$

From this, we can solve for $\frac{\partial \tilde{y}}{\partial x}$:

$$\frac{\partial \tilde{y}}{\partial x} = -\frac{f + xf_x - yg_x}{xf_y - g - yg_y}.$$

Using this expression, we can rewrite the determinant, $Det(J)$:

$$Det(J) = (xf_y - G - yg_y)y\left[-\frac{\partial \tilde{y}}{\partial x}\left(\frac{\partial F}{\partial g}g_y + \frac{\partial F}{\partial y}\right) - \left(\frac{\partial F}{\partial g}g_x + \frac{\partial F}{\partial x}\right)\right].$$

Note that the first multiplier in the parentheses in the expression for $Det(J)$ is negative. Therefore, a necessary stability condition for solution $(x^{(1)}, y^{(1)})$ is given by

$$\frac{\partial \tilde{y}}{\partial x}\left(\frac{\partial F}{\partial g}g_y + \frac{\partial F}{\partial y}\right) + \left(\frac{\partial F}{\partial g}g_x + \frac{\partial F}{\partial x}\right) \geq 0. \tag{16}$$

The dependence of the steady state victim level, $x^{(1)}$, on K. The steady-state level of $x = x^{(1)}$ is defined implicitly by equation (15). To determine the sign of $dx^{(1)}/dK$, let us differentiate equation (15) with respect to K. We obtain:

$$\frac{\partial F}{\partial g}\left(g_x\frac{dx^{(1)}}{dK}+g_y\frac{\partial\tilde{y}}{\partial x}\frac{dx^{(1)}}{dK}+g_y\frac{\partial\tilde{y}}{\partial K}+g_K\right)+\frac{\partial F}{\partial x}\frac{dx^{(1)}}{dK}+\frac{\partial F}{\partial y}\left(\frac{\partial\tilde{y}}{\partial K}+\frac{\partial\tilde{y}}{\partial x}\frac{dx^{(1)}}{dK}\right)=0,$$

where all the derivatives are taken at the point $x^{(1)}, \tilde{y}(x^{(1)}, K)$. This can be rewritten as

$$\frac{dx^{(1)}}{dK}\left[\frac{\partial\tilde{y}}{\partial x}\left(\frac{\partial F}{\partial g}g_y+\frac{\partial F}{\partial y}\right)+\left(\frac{\partial F}{\partial g}g_x+\frac{\partial F}{\partial x}\right)\right]=-\left[\frac{\partial F}{\partial g}\left(g_y\frac{\partial\tilde{y}}{\partial K}+g_K\right)+\frac{\partial F}{\partial y}\frac{\partial\tilde{y}}{\partial K}\right]. \tag{17}$$

Note that the expression in the square brackets in the left hand side of this equation appears in the stability condition for the steady state, inequality (16), and is nonnegative. Therefore the sign of $dx^{(1)}/dK$ coincides with the sign of the right hand side of equation (17). To proceed, we need to determine the sign of the derivative, $\frac{\partial\tilde{y}}{\partial K}$.

Dependence of the function $\tilde{y}(x, K)$ on the carrying capacity. First, let us consider the function $\gamma(x, y)$, and determine its dependence on its variables. This function is given implicitly by equation (13). Let us differentiate equation (13) with $G(x, y, K) = \gamma(x, y)$ with respect to y:

$$\frac{\partial F}{\partial g}\frac{\partial\gamma}{\partial y}+\frac{\partial F}{\partial y}=0\Rightarrow\frac{\partial\gamma}{\partial y}=-\frac{\partial F}{\partial y}\Big/\frac{\partial F}{\partial g}.$$

At this point let us make an additional assumption on the numerical response function F:

$$\frac{\partial F}{\partial y}\leq 0.$$

Then we have the following inequality:

$$\frac{\partial\gamma}{\partial y}\geq 0. \tag{18}$$

The next step is to determine the dependence of $\tilde{y}(x, K)$ on K. The function $\tilde{y}(x, K)$ is given implicitly by equation (14). Let us differentiate this equation

with respect to K:

$$x\left(f_y\frac{\partial\tilde{y}}{\partial K}+f_K\right)-\frac{\partial\tilde{y}}{\partial K}\gamma-\tilde{y}\frac{\partial\gamma}{\partial y}\frac{\partial\tilde{y}}{\partial K}=0.$$

From this we obtain,

$$\frac{\partial\tilde{y}}{\partial K}\left[xf_y-\gamma-\frac{\partial\gamma}{\partial y}\right]=-xf_K.$$

The expression in the square brackets on the left hand side is negative because of the inequality (18), and the right hand side is negative. We conclude that

$$\frac{\partial\tilde{y}}{\partial K}>0.$$

Conditions for a positive correlation between the steady-state victim level and the carrying capacity. The sign of the derivative $dx^{(1)}/dK$ is given by the right-hand side of equation (17),

$$\frac{dx^{(1)}}{dK}\propto-\left[\frac{\partial F}{\partial g}\left(g_y\frac{\partial\tilde{y}}{\partial K}+g_K\right)+\frac{\partial F}{\partial y}\frac{\partial\tilde{y}}{\partial K}\right].$$

The following sufficient condition for the positivity of $dx^{(1)}/dK$ can be formulated: if

$$\frac{\partial F}{\partial g}>0,\quad \frac{\partial F}{\partial y}\leq 0, \tag{19}$$

then condition

$$g_y\frac{\partial\tilde{y}}{\partial K}+g_K<0 \tag{20}$$

guarantees that $dx^{(1)}/dK>0$. In particular, we have two important examples:

- The exploitation function is independent of the number of enemies, and it is negatively correlated with the carrying capacity:

  $$\frac{\partial g}{\partial y}=0 \text{ and } \frac{\partial g}{\partial K}<0. \tag{21}$$

  An example of such a law is given on page 2 of this document, see model (1) of exploitation function. In general, this case corresponds to the situation where the exploitation function scales with the density of the victims, rather than with their total number [3].

- The exploitation function is independent of the carrying capacity, and it is negatively correlated with the number of enemies:

$$\frac{\partial g}{\partial y} < 0 \text{ and } \frac{\partial g}{\partial K} = 0. \tag{22}$$

  Biologically, this can be interpreted as interference/competition among enemies [2, 5, 15], or as frequency-dependent transmission in epidemiology [3]. An example of such a law is given on page 2 by model (2) of exploitation function.

Conditions (21) or (22) guarantee the positivity of $dx^{(1)}/dK$. Note that assumptions (19) are consistent with the examples given in [1]. Further note that we do not have to make any assumptions about the dependence of F on the function x.

Finally we emphasize that in some (exotic) examples of the victim growth rate and the exploitation function, the conditions above may not guarantee that the mass-action model promotes coexistence. Condition (20), although enough to ensure that $dx^{(1)}/dK > 0$, may not lead to a significant extension of the region $x^{(1)} > 1$ for larger values of K. Further, and more subtle, conditions are required to guarantee that. We have however not found any biologically relevant examples where such further conditions would be necessary.

6 Turing instability

It has been observed before [9] that Turing instability [17] can destroy coexistence equilibria in spatially-distributed systems. In this section we demonstrate that the effect we report in the present paper is not of the same nature. In other words, the destabilization of coexistence solution in spatially-extended systems reported here is not caused by Turing instability.

Consider system (1-2), where the carrying capacity, K, corresponds to the mass-action model. Suppose that the system possesses an internal equilibrium, $(x^{(1)}, y^{(1)})$. Consider the stability of this equilibrium by writing down the Jacobian of system (1-2) evaluated at this solution:

$$A = \begin{pmatrix} a_{11} & a_{12} \\ a_{21} & a_{22} \end{pmatrix}.$$

The eigenvalues of this system satisfy the equation,

$$\lambda^2 - \lambda Tr(A) + Det(A) = 0.$$

The solution is stable if the following conditions are satisfied:

$$Tr(A) < 0, \quad (23)$$
$$Det(A) > 0. \quad (24)$$

As mentioned before, adding spatial constraints to this system can be implemented by presenting it as a metapopulation model, which amounts to two changes:

- The system is split into a number of patches, such that the rules specified by equations (1-2) apply in each patch except the value K now corresponds to a smaller, local carrying capacity, $K \rightarrow K_{patch}$.
- The individual patches communicate with each other, which requires additional parameters, m_x and m_y, related to the diffusion coefficients for the two species.

Now, the model can be approximated by the following PDEs:

$$\dot{x} = rx\tilde{f}(x, y, K_{patch}) - \beta y\tilde{g}(x, y, K_{patch}) + D_x\Delta x, \quad (25)$$
$$\dot{y} = \beta y\tilde{g}(x, y, K_{patch}) - ay + D_y\Delta y. \quad (26)$$

Here, the diffusion coefficients $D_x = m_x h^2$ and $D_y = m_y h^2$ are related to the migration rates by means of the scaling factor, h, describing the distance between neighboring patches. Note that there is a number of ways in which the functions $\tilde{f}$ and $\tilde{g}$ change with the carrying capacity K. For example, in Model 1, K can be scaled out and the functions $\tilde{f}$ and $\tilde{g}$ only depend on the *densities*, x/K and y/K, and not on the absolute numbers of the two species. The stability condition for the coexistence solution in this case is simply

$$\frac{a}{\beta} < 1,$$

that is, it is the same in individual patches as it is in the full mass-action system. In other cases (e.g. models 2-4), we can assume that the parameters ϵ and η scale with K, or that they remain constant as K changes. These choices have to be dictated by the particular biological properties of the

underlying models. In this paper we kept parameters ϵ and η independent of K. As a result, the stability properties of the coexistence solution change with K. More precisely, a stability condition for coexistence solutions in models 2 and 4 is

$$\frac{a}{\beta} < \frac{K}{K+\epsilon},$$

that is, for smaller values of K the coexistence region was slightly smaller. However in practical terms, since $\epsilon \ll K$ for both the mass-action and metapopulation models, the shift in the stability line is negligible.

In the analysis below we assume that the coexistence solution remains stable in each of the patches of the spatially-distributed system, that is, inequalities (23-24) hold with the carrying capacity K_{col}. Following the usual procedure, we present a perturbation as a sum of Fourier components, and study the stability properties of each component with frequency q. The modified Jacobian matrix is given by

$$A_q = A - \begin{pmatrix} D_x q^2 & 0 \\ 0 & D_y q^2 \end{pmatrix}.$$

In particular,

$$\begin{aligned} Tr(A_q) &= Tr(A) - (D_x + D_y)q^2 < Tr(A_q), & (27) \\ Det(A_q) &= Det(A) - q^2(D_x a_{22} + D_y a_{11}) + D_x D_y q^4. & (28) \end{aligned}$$

If $Tr(A) < 0$, then adding spatial effects cannot reverse this inequality. To find out whether the new determinant can be negative, we note that the minimum of the expression $Det(A_q)$ is achieved for

$$q^2 = q_m^2 = \frac{a_{22}D_x + a_{11}D_y}{2D_x D_y}.$$

If however the expression for q_m^2 is negative, the minimum is achieved at $q = 0$ (that is, in the absence of a spatial structure). Thus Turing instability takes place only if

$$a_{22}D_x + a_{11}D_y > 0. \quad (29)$$

If the condition $D_x = D_y$ holds, then the above inequality is impossible because of the stability condition (23). Therefore, the observed enlargement of the coexistence region in the mass-action systems is not a result of a Turing instability.

In the case where $D_x \neq D_y$, a necessary condition for Turing instability (29) can be satisfied, and the existence of a Turing instability cannot be excluded. However, in such cases the Turing instability would shift the stability line ($a/\beta \approx 1$ in all 4 models presented here), thus making the upper boundary of the coexistence region in spatially-extended systems shift downward. This is very different from the phenomenon reported here, where the *lower* boundary of the coexistence region is shifted upward in spatial models.

References

[1] Abrams, P.A. and Ginzburg, L.R. (2000) The nature of predation: prey dependent, ratio dependent or neither? Trends in Ecology & Evolution 15, 337–341.

[2] Beddington, J.R. (1975) Mutual interference between parasites or predators and its effect on searching efficiency. J. Anim. Ecol. 44, 331–430.

[3] Begon, M., Bennett, M., Bowers, RG, French, NP, Hazel, SM, Turner, J. and others (2002) A clarification of transmission terms in host-microparasite models: numbers, densities and areas. Epidemiology and Infection 129, 147–153.

[4] Boots, M. and Sasaki, A. 2002. Parasite-Driven Extinction in Spatially Explicit Host-Parasite Systems. The American Naturalist 159, 706–713.

[5] DeAngelis, D.L., Goldstein, R.A., and O'Neil, R.V. (1975) Model for trophic interaction. Ecology 56, 881–892.

[6] De Carvalho, K.C. and Tome, T. 2007. Stable oscillations of a predator-prey probabilistic cellular automaton: a mean-field approach. J. Phys. A: Math. Theor. 40, 12901–12915.

[7] Gillespie, D.T. (1976). A general method for numerically simulating the stochastic time evolution of coupled chemical reactions. J. Comp. Phys., 22, 403–434.

[8] Gillespie, D.T. (1977). Exact stochastic simulation of coupled chemical reactions. J. Phys. Chem., 81, 2340–2361.

[9] Levin, S.A. (1974) Dispersion and population interactions. Am. Nat. 108, 207–228.

[10] Lloyd, A.L. (2004). Estimating variability in models for recurrent epidemics: assessing the use of moment closure techniques. Theor. Pop. Biol. 65, 49–65.

[11] McCallum, H., Barlow, N., and Hone, J. (2001) How should pathogen transmission be modelled? Trends Ecol Evol 16, 295–300.

[12] Rand, D.A. Correlation Equations and Pair Approximations for Spatial Ecologies. 1999. CWI Quarterly 12, 329–368.

[13] Sato, K., Matsuda, H. and Sasaki, A. 1994. Pathogen invasion and host extinction in lattice structured populations. J. Math. Biol. 32, 251–268.

[14] Satulovsky, J.E. and Tome, T. 1994. Stochastic lattice gas model for a predator-prey system. Phys. Rev. E 49, 5073–5080.

[15] Skalski, G.T. and Gilliam, J.F. (2001) Functional responses with predator interference: viable alternatives to the Holling type II model. Ecology 82, 3083–3092.

[16] Sun, Z., Wodarz, D. and Komarova, N.L. 2011. On the accuracy of analytic approximations to agent-based natural enemy models. In preparation.

[17] Turing, A. (1952). The chemical basis of morphogenesis. Phil. Trans. R. Soc. London, 237–72.